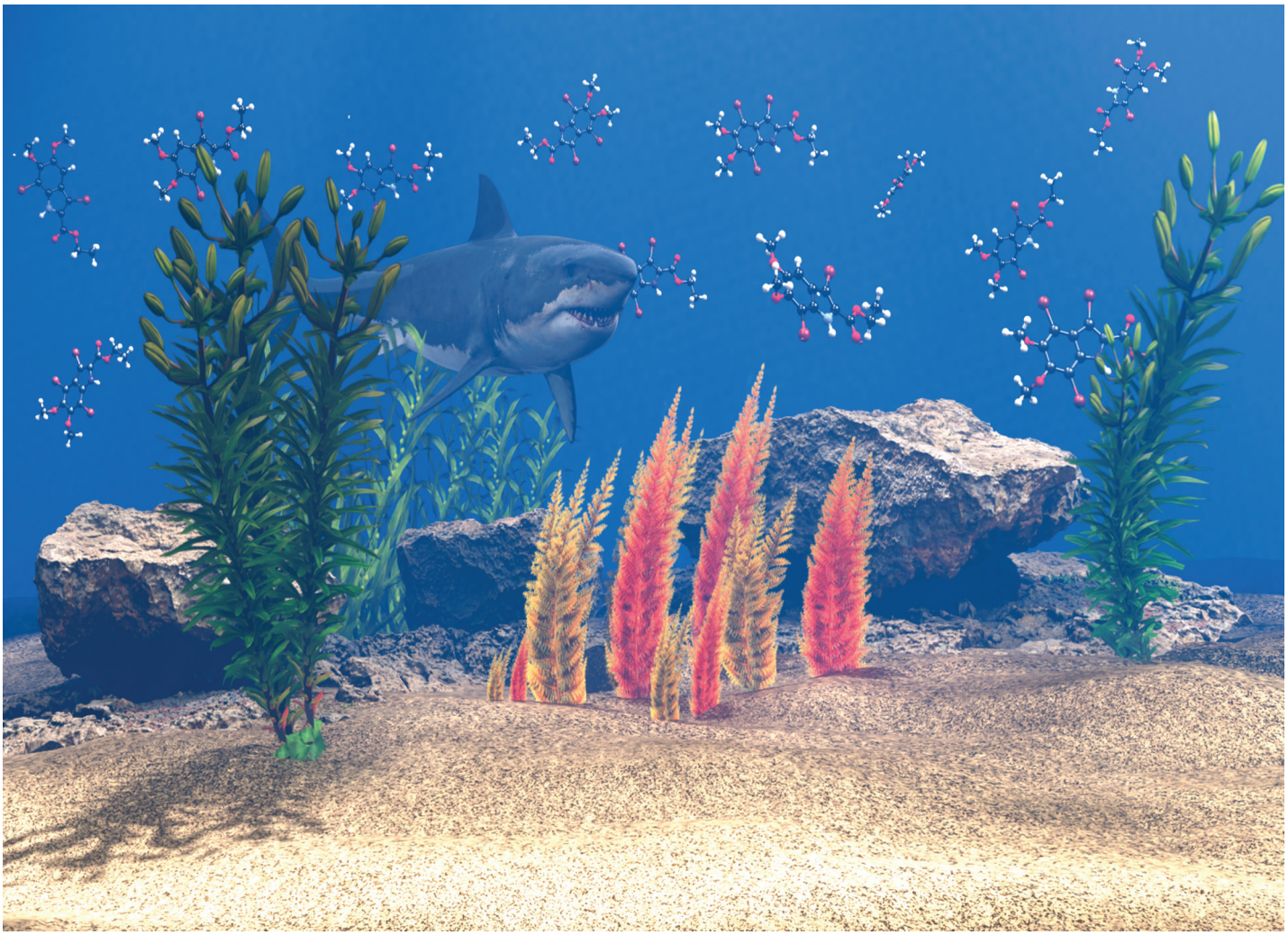

Showcasing research from Professor Mahesh Hariharan's laboratory, School of Chemistry, Indian Institute of Science Education and Research Thiruvananthapuram (IISER TVM), Kerala, India.

Probing intersystem crossing in multi-brominated eumelanin through transient absorption and surface hopping dynamics

The ultrafast dynamics of di-brominated and tri-brominated eumelanin monomers are investigated through pump-probe spectroscopy and surface hopping including arbitrary couplings (SHARC) approach.

Cover art created by Lukhmanul Hakeem K.

As featured in:

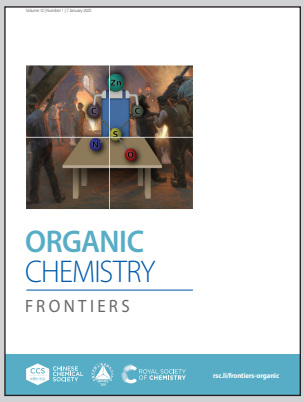

See Mahesh Hariharan *et al.*, *Org. Chem. Front.*, 2025, **12**, 33.

CCS 中国化学会 CHINESE CHEMICAL SOCIETY
SIOC 1950
ROYAL SOCIETY OF CHEMISTRY
rsc.li/frontiers-organic

ORGANIC CHEMISTRY FRONTIERS

RESEARCH ARTICLE

View Article Online
View Journal | View Issue

Cite this: *Org. Chem. Front.*, 2025, **12**, 33

Probing intersystem crossing in multi-brominated eumelanin through transient absorption and surface hopping dynamics†

Kavya Vinod, ‡ Lukhmanul Hakeem K., ‡ Diana Thomas, Pallavi Panthakkal Das and Mahesh Hariharan *

Achieving intersystem crossing (ISC) through structural tuning in biological systems is an evolving area for therapeutic and materials research. Eumelanin, a natural pigment, offers huge potential for bio-inspired material design, yet remains underexplored in this regard. Herein, we report the ultrafast intersystem crossing in di-brominated (DMICE-Br_2) and tri-brominated (DMICE-Br_3) eumelanin model monomers through transient absorption spectroscopy and surface hopping dynamics. Femtosecond and nanosecond transient absorption experiments suggest triplet excited state populations in DMICE-Br_2 and DMICE-Br_3 with triplet quantum yields and rates of ISC as $\phi_T^{DMICE\text{-}Br_2} = 30.2\%$, $k_{ISC}^{DMICE\text{-}Br_2} = 4.37 \times 10^{10}\ s^{-1}$ and $\phi_T^{DMICE\text{-}Br_3} = 42.1\%$, $k_{ISC}^{DMICE\text{-}Br_3} = 1.09 \times 10^{11}\ s^{-1}$ respectively. Theoretical insights into ISC were obtained with nonadiabatic dynamics simulations using the surface hopping including arbitrary couplings method coupled to potential energy surfaces, modelled by linear vibronic coupling (SHARC/LVC). The results show that for both DMICE-Br_2 and DMICE-Br_3, the initial S_1 population decays to the T_2 and T_3 states in the picosecond timescale to further undergo internal conversion to T_1 within sub-ns for DMICE-Br_2 and sub-ps for DMICE-Br_3. The simulated $k_{ISC}^{DMICE\text{-}Br_2} = 4.73 \times 10^{10}\ s^{-1}$ and $k_{ISC}^{DMICE\text{-}Br_3} = 4.13 \times 10^{11}\ s^{-1}$ corroborate to the assignment of the ultrafast triplet excited state population observed in the experiments. The increased triplet yields and ISC rates in DMICE-Br_2 and DMICE-Br_3 are attributed to the enhanced heavy atom effect from additional bromine atoms. This work presents the experimental and computational evidence for ultrafast ISC in multi-brominated eumelanin monomers, with promising implications for eumelanin-inspired material design and photodynamic applications.

Received 30th September 2024,
Accepted 8th November 2024

DOI: 10.1039/d4qo01832j

rsc.li/frontiers-organic

Introduction

Intersystem crossing (ISC) is the non-radiative, spin-forbidden transition between two electronic states of different multiplicities.[1,2] Recently, ISC in biological molecules and the resultant photochemistry have drawn increased attention due to their potential use in clinical research.[3,4] In photoactive bio-inspired molecules, ISC can be involved in the generation of reactive oxygen species (ROS) which contributes to photodamage in cells, enabling its use in photodynamic therapy.[5,6] For such applications, structural modifications of biomolecules especially by heavy atom incorporation can induce ISC with good yields.[7,8] Tracking the excited state dynamics of synthetic bio-inspired photosensitizers is a necessity to guarantee their efficiency, especially since numerous photophysical and photochemical transformations may occur within ultrafast timescales upon photoexcitation.[9] The high degrees of freedom and the large number of electronic excited states in these molecules contribute to the availability of different decay pathways.[10] In this regard, a combination of ultrafast spectroscopy and theoretical simulations is ideal to investigate the excited state species and the intricate decay modes in small bio-organic molecules. The exploration of potential energy surfaces (PESs) of organic molecules with stationary quantum chemistry is a well-established research field,[11–13] but transient absorption experiments coupled with nonadiabatic dynamics simulations are relatively rarer.[14–16] Recently, the ultrafast excited-state deactivation mechanism of 6-selenoguanine in water was investigated using femtosecond transient absorption and nonadiabatic trajectory surface-hopping dynamics to conclude that ISC and internal conversion (IC) channels are involved in the energy deactivation of the selenium incorporated nucleobase.[17,18]

School of Chemistry, Indian Institute of Science Education and Research Thiruvananthapuram (IISER TVM), Maruthamala P.O., Vithura, Thiruvananthapuram 695551, Kerala, India. E-mail: mahesh@iisertvm.ac.in

†Electronic supplementary information (ESI) available. CCDC 2387375 and 2387376. For ESI and crystallographic data in CIF or other electronic format see DOI: https://doi.org/10.1039/d4qo01832j

‡These authors contributed equally.

Eumelanin, a natural bio-pigment, has intrigued researchers due to its unique structural and optoelectronic properties.[19,20] Two key monomers of eumelanin, 5,6-dihydroxyindole (DHI) and 5,6-dihydroxyindole-2-carboxylic acid (DHICA), play a pivotal role in its structure.[21–23] Recent research on eumelanin and eumelanin-inspired materials positions them as a novel and versatile class with potential applications in both medical and materials science.[24,25] The photochemistry of biologically relevant molecules such as DNA nucleobases upon heavy atom substitution enables their use in photodynamic therapy due to the high triplet yields.[17,26] Eumelanin monomers have been underexplored in this context, though halogenation can improve their triplet quantum yields, positioning them as potential candidates for photodynamic therapy alongside DNA monomers and chlorophyll analogues.[17,26,27] Our recent work on halogenated eumelanin model monomers revealed ultrafast ISC for mono-brominated (DMICE-Br) and mono-iodinated eumelanin monomers in solution and room temperature phosphorescence in the mono-iodinated monomer in the crystalline state.[23] Our ongoing efforts to monitor the photogenerated excitons[23,28–30] and delve deeper into ISC in eumelanin monomers prompted us to introduce multiple bromine atoms into the protected eumelanin monomer, ethyl 5,6-dimethoxyindole-2-carboxylate (DMICE), to yield DMICE-Br_2 and DMICE-Br_3. The experimental and theoretical results indicate that increasing the number of bromine substitutions in DMICE leads to higher rates of intersystem crossing (ISC) and greater triplet quantum yields, thereby enhancing the overall ISC efficiency in the order of DMICE-Br_3 > DMICE-Br_2 > DMICE-Br. The observed photophysics of the multi-brominated eumelanin monomers has broader implications in prospective photomedicine and materials science research.

Results and discussion

The brominated derivatives of DMICE, that is, DMICE-Br_2 and DMICE-Br_3, were synthesized according to previously reported procedures and characterized as per standard analytical techniques.[31] Bromination of DMICE using *N*-bromosuccinimide (NBS) at 65 °C in tetrahydrofuran for 2 hours and in acetonitrile for 24 hours resulted in DMICE-Br_2 and DMICE-Br_3, respectively, in good yields (Fig. 1 and Schemes S1, S2†). Slow evaporation of DMICE-Br_2 and DMICE-Br_3 solutions separately in an ethyl acetate/hexane solvent mixture at room temperature yielded good quality colourless single crystals for X-ray crystallography. DMICE-Br_2 and DMICE-Br_3 crystallized in monoclinic crystal systems with $P2_1/c$ and $C2/c$ space groups respectively (Fig. S1–S3 and Table S1†). On analysing the crystal packing of DMICE-Br_2 and DMICE-Br_3, hydrogen bonding, π–π interactions and bromine interactions were identified. The Hirshfeld surface analyses performed on the crystal structures quantified the major stabilizing non-covalent interactions to be H···H (35.6% in DMICE-Br_2 and 29.7% in DMICE-Br_3), Br···H (23.3% in DMICE-Br_2 and 30.5% in DMICE-Br_3), O···H (16.8% in DMICE-Br_2 and 15.5% in DMICE-Br_3), C···C (4.9% in DMICE-Br_2 and 7.6% in DMICE-Br_3), Br···Br (4.5% in DMICE-Br_3) and C···H (7.9% in DMICE-Br_2) (Fig. S4, S5 and Table S2†).[32,33] Symmetry-adapted perturbation theory (SAPT (0)) was performed on the identified dimer orientations of DMICE-Br_2 and DMICE-Br_3 to quantitatively elucidate the different non-covalent interactions (electrostatic, exchange, induction, and dispersion) stabilizing the crystal packing (Tables S3 and S4†).[34] Co-facial orientations of DMICE-Br_2 and DMICE-Br_3 were identified as the most stable molecular orientations within the respective crystal packings due to the prominent dispersion interactions within the assemblies. Non-covalent interactions (NCI) index analysis also revealed that the green iso-surfaces were prominent for the co-facial orientations of DMICE-Br_2 and DMICE-Br_3, signifying energy stabilization within these orientations in the crystal packings (Fig. S6 and S7†).[35,36]

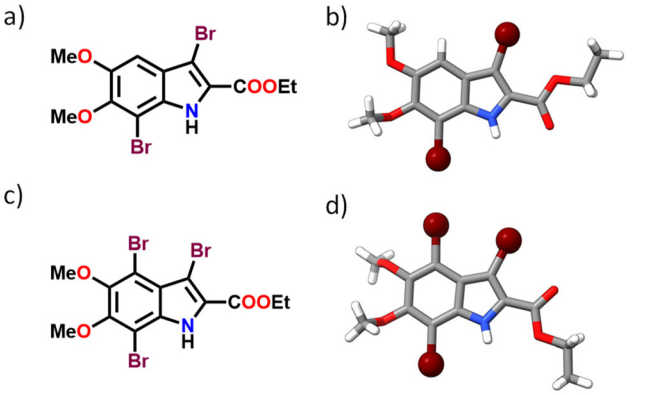

Fig. 1 (a) Molecular structure of DMICE-Br_2, (b) crystal structure of DMICE-Br_2, (c) molecular structure of DMICE-Br_3 and (d) crystal structure of DMICE-Br_3.

The primary photophysical properties of DMICE-Br_2 and DMICE-Br_3 were investigated using steady-state UV-vis absorption and fluorescence emission spectroscopy in toluene at room temperature (Fig. 2). The UV-vis absorption spectra of DMICE-Br_2 and DMICE-Br_3 displayed minimal differences with respect to each other with absorption maxima at 307 nm and 308 nm respectively. The fluorescence emission maximum of DMICE-Br_2 was observed at 378 nm and that for DMICE-Br_3 at 390 nm, with a red-shift of $\Delta\lambda$ = 12 nm compared to DMICE-Br_2. The non-brominated eumelanin monomer DMICE exhibited UV-vis absorption maximum at 325 nm and fluorescence emission maximum at 365 nm as reported earlier from our group.[23] The fluorescence quantum yields estimated through a relative method in toluene drastically decreased with the increase in the number of bromine atoms from Φ_f = 49.3% in non-brominated DMICE to Φ_f = 3.5% in DMICE-Br to Φ_f < 1% in both DMICE-Br_2 and DMICE-Br_3.[23] The significant reduction of the fluorescence emission with the incorporation of a greater number of bromine atoms in the eumelanin monomer indicates that upon multi-bromination, alternate non-radiative decay pathways become more efficient rather than fluorescence.[2,23,37,38]

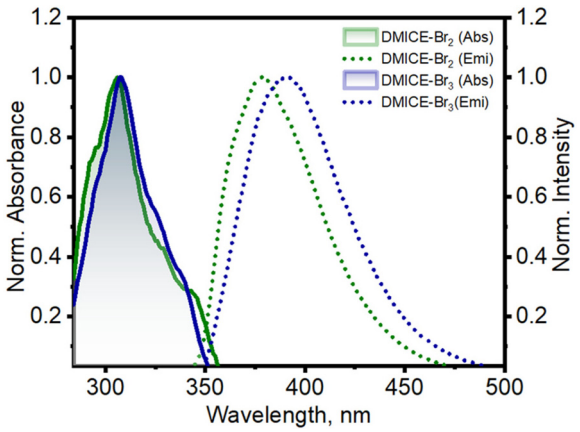

Fig. 2 Normalized UV-vis absorption and fluorescence emission spectra of DMICE-Br_2 and DMICE-Br_3 in toluene.

To examine the excited-state relaxation mechanisms leading to efficient non-radiative decay in multi-brominated eumelanin monomers, femtosecond transient absorption (fsTA) measurements were performed. A Spectra-Physics Tsunami oscillator (80 MHz, 800 nm) served as the seed for a Spectra-Physics Spitfire regenerative amplifier (1 kHz, 4 mJ). A portion of the amplified output was utilized to produce a 400 nm pump pulse, while the remaining 800 nm pulse was directed through a delay line within an ExciPro pump–probe spectrometer. To generate the white light continuum from the delayed 800 nm pulses, a rotating 2 mm thick CaF_2 plate was used. Fig. 3 displays the fsTA spectra and the corresponding deconvoluted spectra for DMICE-Br_2 and DMICE-Br_3 in toluene. Following photoexcitation of DMICE-Br_2 at λ_{exc} = 325 nm (O.D. at λ_{exc} = 0.3) with a 100 fs pump pulse, a broad positive absorption feature appears between 470 and 770 nm, similar to the broad singlet absorption previously observed in DHICA as well as DMICE.[23,39] As the broad singlet excited state decays, DMICE-Br_2 reveals a sharp additional peak around ~520 nm within a few tens of picoseconds (Fig. 3a). The new spectral signature in DMICE-Br_2 at the later time delays resembles that of the triplet excited species previously reported for DMICE-Br.[23] The evolution-associated spectra (EAS) for DMICE-Br_2 and DMICE-Br_3 were generated using global fitting of the fsTA data in a time *versus* wavelength framework, modelled as an A → B → GS (GS = ground state) sequential process. Selected kinetic traces with global analysis fitted curves at different wavelengths are shown in Fig. S8† to illustrate the quality of the fits.

Upon spectral deconvolution, two distinct components emerge from the fsTA data for DMICE-Br_2. The first component (A) is attributed to the singlet state, with a decay time

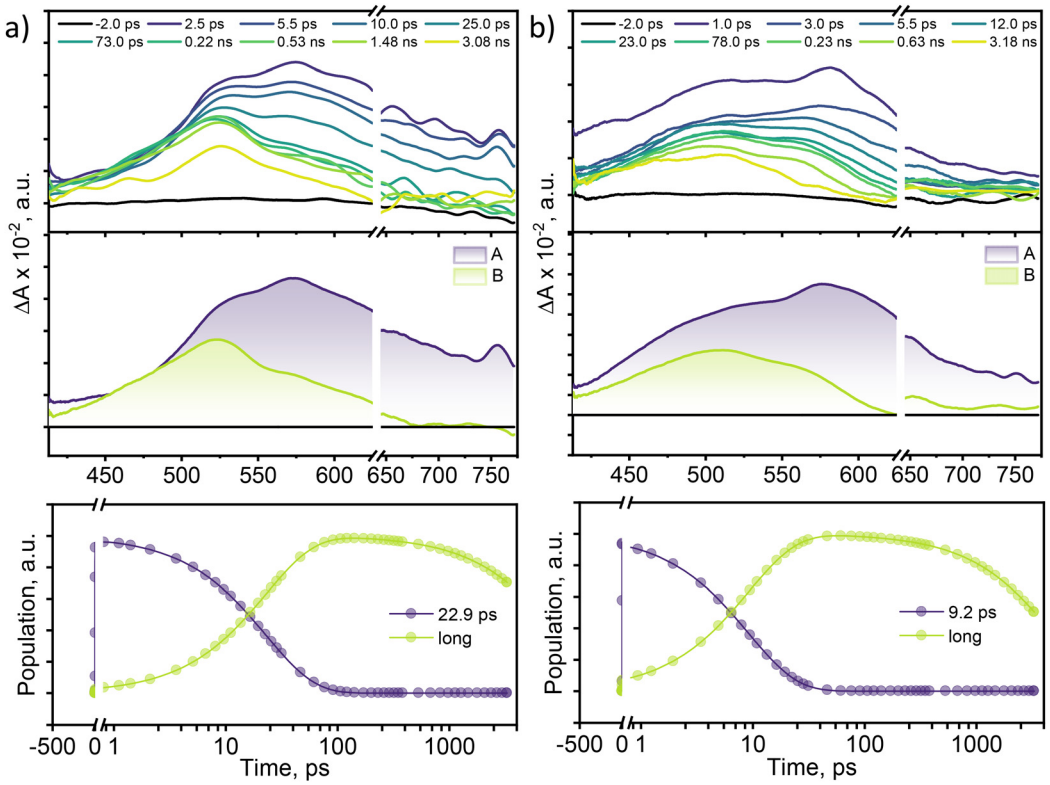

Fig. 3 (Top) Femtosecond transient absorption spectra of (a) DMICE-Br_2 and (b) DMICE-Br_3 in toluene; (middle) evolution-associated spectra (EAS) obtained from the deconvolution of the total spectra through global analysis; (bottom) kinetic profiles of the deconvoluted plots fitted through global analysis using the A → B → GS sequential model.

constant of $\tau_{A\rightarrow B}$ = 22.9 ps. The second component (B), which is blue-shifted by 50 nm relative to component A, is long-lived and persists beyond the 3.5 ns experimental window. The fsTA spectra for DMICE-Br_3 in toluene also revealed the initial broad spectra upon photoexcitation, ranging from 420–750 nm. The initial broad species decay in a few picoseconds to populate another species with a spectral signature of around 420–600 nm and blue-shifted by 69 nm with respect to the initial spectral traces (Fig. 3b). The lack of an isosbestic point in the fsTA spectral traces of DMICE-Br_2 and DMICE-Br_3 may be attributed to the overlap between the singlet and triplet signatures in the brominated eumelanin counterparts. The deconvolution of the total spectra reveals that component A (singlet species) decays within $\tau_{A\rightarrow B}$ = 9.2 ps to populate component B which is a long-lived species and persists across the experimental delay line. The rate of formation of the non-decaying species in DMICE-Br_2 and DMICE-Br_3 is different suggesting the impact of the number of bromine atoms in determining the rate of the singlet decay in the respective molecule. In our previous work on the mono-brominated eumelanin monomer (DMICE-Br), we reported the singlet state decay followed by triplet excited state formation in DMICE-Br within 0.13 ns.[23] On the other hand, the non-brominated DMICE revealed singlet decay within 3.62 ns with negligible ISC.[23] The long-lived species observed in the multi-brominated eumelanin monomers could be triplet manifolds formed from intersystem crossing.

To investigate the nature of long-lived species observed in the femtosecond transient absorption (fsTA) experiments of DMICE-Br_2 and DMICE-Br_3, we performed nanosecond transient absorption measurements (nsTA) in toluene. The photoexcitation of DMICE-Br_2 and DMICE-Br_3 at 355 nm (pulse width ≈ 8 ns) produces a positive excited state absorption (ESA) band in the nitrogen-purged solution, ranging from 440–550 nm in DMICE-Br_2 and 380–600 nm in DMICE-Br_3 (Fig. S9 and S10†). To confirm and quantify the formation of the triplet excited state, we performed triplet–triplet energy transfer experiments from DMICE-Br_2 and DMICE-Br_3 to beta-carotene as the triplet acceptor, using [Ru(bpy)$_3$]Cl_2 as the reference.[23] The decay rates of the triplet excited state in DMICE-Br_2, DMICE-Br_3, and [Ru(bpy)$_3$]Cl_2 without the addition of beta-carotene were measured. Subsequently, after the addition of beta-carotene, the triplet excited state growth rates at 540 nm were monitored in DMICE-Br_2 and DMICE-Br_3 relative to [Ru(bpy)$_3$]Cl_2 (Fig. S11 and S12†). The triplet quantum yields measured in toluene show the increase in triplet population from Φ_T = 30.2% in DMICE-Br_2 to Φ_T = 42.1% in DMICE-Br_3.[23] Experimental results show that DMICE-Br_2 exhibits a rate of ISC of k_{ISC} = 4.37×10^{10} s^{-1} while DMICE-Br_3 shows an increase in the rate of ISC with $k_{ISC} = 1.09 \times 10^{11}$ s^{-1}. Previously, we reported the triplet quantum yield and rate of ISC (k_{ISC}) of DMICE-Br to be Φ_T = 25.4% and $k_{ISC} = 1.95 \times 10^9$ s^{-1}, respectively, while for DMICE, $\Phi_T \approx 0$.[23] This trend of ISC rates and triplet quantum yields of DMICE ≪ DMICE-Br < DMICE-Br_2 < DMICE-Br_3 could be due to the enhanced heavy atom effect, caused by the increase in the number of bromine atoms from DMICE to DMICE-Br_3.

Having established the intersystem crossing channels for DMICE-Br_2 and DMICE-Br_3, we performed delayed emission experiments for the multi-brominated compounds to examine the non-radiative/radiative nature of the triplet excited states in solution. Delayed emission experiments were performed at room temperature as well as 77 K at a delay time of 0.05 ms upon excitation at λ_{exc} = 310 nm in toluene. At room temperature, delayed emission was not observed in either DMICE-Br_2 or DMICE-Br_3. On the other hand, at 77 K, vibronically resolved delayed emission spectra were observed for both DMICE-Br_2 and DMICE-Br_3 (Fig. S13a†). The delayed emission spectrum of DMICE-Br_2 ranges from 460–630 nm and that of DMICE-Br_3 ranges from 477–650 nm. A red-shift of $\Delta\lambda$ = 19 nm in the gated emission spectra of DMICE-Br_3 with respect to DMICE-Br_2 was observed. Also, the gated emission spectrum of DMICE-Br_2 demonstrates a bathochromic shift of $\Delta\lambda$ = 105 nm with respect to the prompt fluorescence. Similarly, DMICE-Br_3 displays a bathochromic shift of $\Delta\lambda$ = 112 nm between the gated emission and prompt fluorescence. The difference in the emission maxima between the prompt and delayed emission suggests that phosphorescence is activated within the multi-brominated molecules at low temperatures.[40] The phosphorescence lifetimes of DMICE-Br_2 and DMICE-Br_3 in de-aerated toluene at 77 K were estimated to be τ_P = 16.27 ± 0.30 ms and 7.65 ± 0.12 ms respectively (Fig. S13b†). Generally, non-radiative transitions are repressed at low temperatures, thus rigidifying molecular conformations and reducing vibrational energy dissipations.[41] Hence, phosphorescence is activated within the multi-brominated chromophores at low temperatures.

To inspect the role of bromine atoms in populating the triplet excited states in the eumelanin monomers, S–T energy gaps and spin–orbit coupling matrix elements were computed, providing critical insights into the ISC mechanism observed experimentally in DMICE-Br_2 and DMICE-Br_3 (Table S5†). The $S_1 \rightarrow T_2$ transition appears to be more favorable, attributed to the relatively smaller S–T energy gap ($\Delta E_{S_1-T_2}$ = 0.68 eV for DMICE-Br_2 and $\Delta E_{S_1-T_2}$ = 0.38 eV for DMICE-Br_3). In contrast, the larger energy gap between the S_1 and T_1 states ($\Delta E_{S_1-T_1} \sim 1$ eV) likely diminishes the probability of a direct $S_1 \rightarrow T_1$ transition. This conclusion is further corroborated by a detailed investigation of the NTOs and electron density difference plots for the S_1 and T_2 states, which validates the ISC mechanism in both compounds (Fig. S14–S17†). In the S_1 state, the Br-centered transition densities exhibit moderate rotational displacement from the indole plane, while the T_2 state predominantly features an indole-centered π–π* character, which likely facilitates the necessary orbital angular momentum change for efficient ISC.

With the aim of further elucidating the origin of the experimental time constants associated with ISC and definitively identifying the dominant relaxation pathways in DMICE-Br_2 and DMICE-Br_3, we performed surface hopping dynamics on DMICE-Br_2 and DMICE-Br_3 using the SHARC/LVC method as

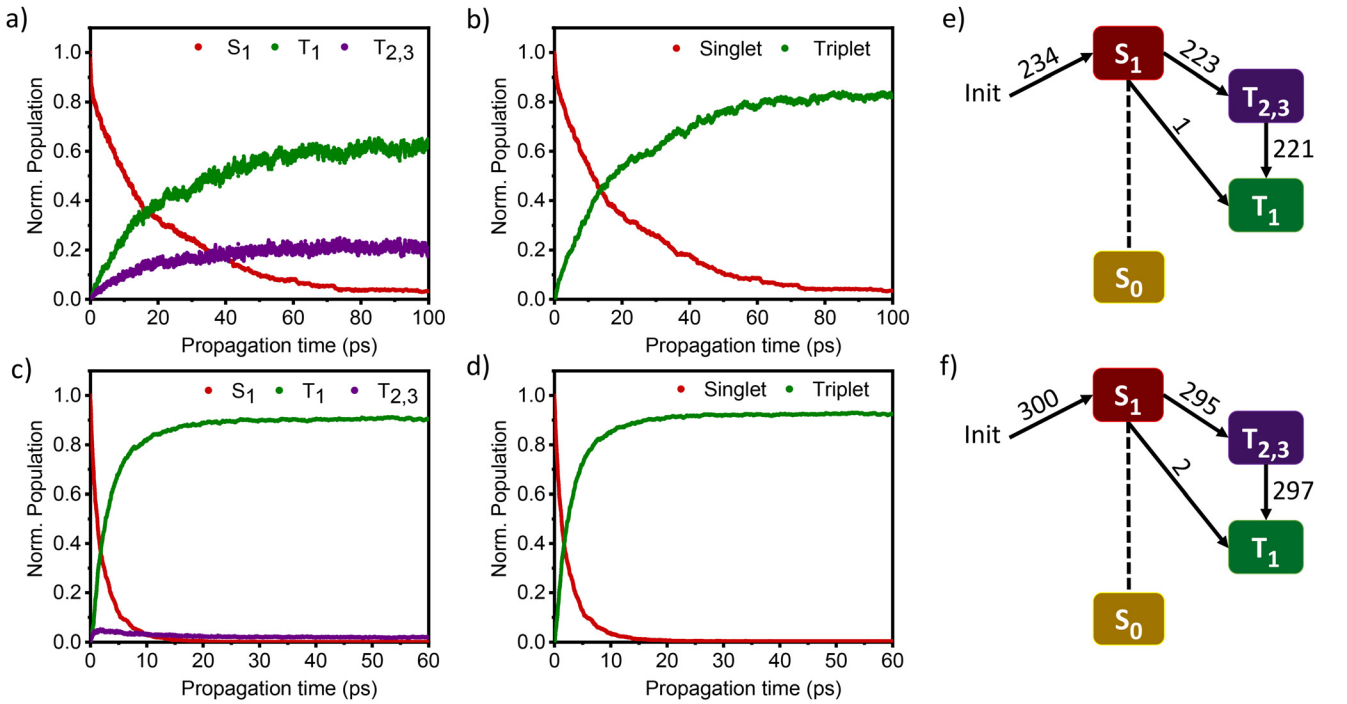

Fig. 4 (a) Time evolution of the excited-state populations of DMICE-Br_2 from an ensemble of 234 trajectories, (b) total singlet and triplet populations in DMICE-Br_2, (c) time evolution of the excited-state populations of DMICE-Br_3 from an ensemble of 300 trajectories, (d) total singlet and triplet populations in DMICE-Br_3, (e) number of net hops in DMICE-Br_2, and (f) number of net hops in DMICE-Br_3. Few trajectory hops were also observed from the S_1 state to the higher triplet excited states, which then underwent internal conversion to the $T_{2,3}$ states (note: Init = initial; Norm. = normalized).

developed by Plasser, González and co-workers (Fig. 4).[42–46] An analytical LVC model was applied to depict the excited-state potential energy surfaces (PESs) of DMICE-Br_2 and DMICE-Br_3. LVC models utilized in SHARC were parametrized as per literature reports.[42] The structures of the multi-brominated compounds were optimized in the singlet ground state, and the subsequent frequency calculations confirmed that all vibrational frequencies were positive. The calculations were performed at the B3LYP/def2-TZVP level of theory and dispersion was incorporated *via* the D3 Becke–Johnson scheme.[47] The impact of solvent was approximately treated with the conductor-like polarizable continuum model (CPCM) with toluene (ε = 2.4, n = 1.497), and all initial calculations were performed using ORCA 5.0.4.[48,49] The normal mode information for both the compounds was extracted from the frequency calculations and transformed into mass-weighted normal modes. To prevent the spurious coupling between the states, the normal modes with ω_i < 300 cm^{-1} were excluded.[50] Among the 93 normal modes, 73 normal modes were considered in order to parametrize the LVC model.[50]

For DMICE-Br_2 and DMICE-Br_3, vertical excitation time-dependent density functional theory (TDDFT) calculations with the TDA-B3LYP functional and def2-TZVP basis set were performed through the SHARC–ORCA interface at the reference geometry and along the selected normal mode coordinates. Dispersion correction was applied using the D3 Becke–Johnson scheme and solvent effects were approximately treated with the CPCM method (toluene, ε = 2.4 and n = 1.497).[51] 10 singlet states (ground state plus 9 excited states) and 10 triplet states were computed. The computed vertical excitation energies in eV and the respective oscillator strengths are given in the ESI (Tables S6 and S7†). For the SHARC/LVC simulations of DMICE-Br_2 and DMICE-Br_3, 3000 initial conditions were derived from the Wigner distribution of the harmonic oscillator of the ground state, based on normal modes and frequencies obtained at the B3LYP/def2-TZVP level of theory.[42,43,52,53] At each of these initial conditions, single-point vertical excitation calculations were carried out using the SHARC/LVC interface. The optical UV-vis absorption spectra of DMICE-Br_2 and DMICE-Br_3 were computed from 3000 initial conditions (Fig. S18†).

The nonadiabatic dynamics simulations of DMICE-Br_2 and DMICE-Br_3 were carried out in the framework of the surface hopping method using the SHARC 3.0 suite of programs, which can include both nonadiabatic coupling and spin–orbit coupling (SOC) simultaneously.[42,43,52,54–56] DMICE-Br_2 and DMICE-Br_3 were excited in the range of 3.50–3.70 eV where the dynamics predominantly started from the S_1 state. For DMICE-Br_2, a total of 234 trajectories were propagated for 100 ps with a time step length of 0.5 fs, and the wavefunctions were propagated by the locally diabatic method.[52,57–59] The simulated excited-state dynamics for DMICE-Br_2 are shown in Fig. 4a, which indicates that the S_1 state is mainly populated at the initial stage. Fig. 4a further shows that the ultrafast decay

of the singlet excited state population leads to the population of the triplet excited state on a picosecond timescale. The relaxation time of the singlet to the triplet for DMICE-Br_2 was derived by fitting a sequential first-order kinetics model to the population data, resulting in a decay time of 21.14 ps, in good agreement with the experimental result.[42] Fig. 4e illustrates that out of the 234 trajectories of DMICE-Br_2, a majority of 223 net hops originate from the S_1 state to the $T_{2,3}$ states. Subsequently, only one net hop occurs from the S_1 state directly to the T_1 state while 221 net hops occur from the $T_{2,3}$ states to the T_1 state. This strongly suggests that DMICE-Br_2 follows $S_1 \rightarrow T_{2,3} \rightarrow T_1$ relaxation as the major energy decay pathway (Table S8†).

The excited state dynamics for DMICE-Br_3 depicted in Fig. 4c also show that the S_1 state is predominantly populated at the initial stage. The ultrafast decay of the singlet excited state results in the rapid growth of the triplet excited states in DMICE-Br_3, when compared to DMICE-Br_2. The faster growth kinetics of the triplet excited state of DMICE-Br_3 is attributed to the enhanced heavy atom effect caused by the higher number of bromine atoms in DMICE-Br_3 as compared to DMICE-Br_2. A total of 300 trajectories were propagated for DMICE-Br_3 with 60 ps duration and 0.5 fs time step length, and the wavefunctions were propagated by the locally diabatic method. The decay time of the singlet to the triplet for DMICE-Br_3 was obtained by fitting a sequential first-order kinetics model to the population data, yielding a value of 2.42 ps, in agreement with the experimental decay time. In the case of DMICE-Br_3, Fig. 4f reveals that out of the hopping dynamics across all 300 trajectories, 295 net hops occur from the S_1 state to the $T_{2,3}$ states, and 2 net hops occur from the S_1 state directly to the T_1 state. Thus DMICE-Br_3 also follows $S_1 \rightarrow T_{2,3} \rightarrow T_1$ deactivation as the major energy relaxation channel (Table S8†). In DMICE-Br_3, the S_1–T_2 crossing geometry exhibits a pronounced non-planar distortion compared to DMICE-Br_2, which may facilitate a more rapid radiationless decay toward the nearest minimum energy conical intersection, which is the T_2–T_1 crossing geometry (Fig. S19 and S20†).[60] The computed k_{ISC} for DMICE-Br_2 and DMICE-Br_3 follows the increasing trend of $k_{ISC} = 4.73 \times 10^{10}$ s^{-1} in DMICE-Br_2 to $k_{ISC} = 4.13 \times 10^{11}$ s^{-1} in DMICE-Br_3 and these values are in good agreement with the experimental results. A difference of nearly one order of magnitude is observed between the k_{ISC} of DMICE-Br_2 and DMICE-Br_3 both experimentally and theoretically. This is due to the additional bromine atom in DMICE-Br_3 compared to DMICE-Br_2 causing an increased heavy atom effect.[61]

Conclusions

In this work, we examine the ultrafast intersystem crossing dynamics of DMICE-Br_2 and DMICE-Br_3 by employing transient absorption spectroscopy and surface hopping simulations. The formation of long-lived species in both DMICE-Br_2 and DMICE-Br_3 was monitored through femtosecond transient absorption experiments. Nanosecond transient absorption measurements further confirmed the long-lived species to be triplet excited states. The increase in the number of bromine atoms from DMICE-Br_2 to DMICE-Br_3 induces a stronger heavy atom effect in DMICE-Br_3 as compared with DMICE-Br_2, which significantly enhances the intersystem crossing (ISC) rate by nearly one order of magnitude from $k_{ISC} = 4.37 \times 10^{10}$ s^{-1} in DMICE-Br_2 to $k_{ISC} = 1.09 \times 10^{11}$ s^{-1} in DMICE-Br_3. Consequently, the singlet state lifetime reduces from $\tau_s = 22.9$ ps in DMICE-Br_2 to $\tau_s = 9.2$ ps in DMICE-Br_3. The increase in k_{ISC} is also accompanied by an increase in triplet quantum yields as the number of bromine atoms increases ($\phi_T^{\text{DMICE-Br}_2} = 30.2\%$ and $\phi_T^{\text{DMICE-Br}_3} = 42.1\%$). The experimental results align with the heavy-atom effect previously observed for DMICE-Br and are now also evident in the current molecules of interest, DMICE-Br_2 and DMICE-Br_3. Surface hopping dynamics simulations using the SHARC/LVC method further reveal the ultrafast ISC in both DMICE-Br_2 and DMICE-Br_3, in agreement with the experimental data. The SHARC/LVC method successfully reproduces the observed trend in the reduction of singlet lifetimes from $\tau_s = 21.14$ ps in DMICE-Br_2 to $\tau_s = 2.42$ ps in DMICE-Br_3. The calculated rates of ISC reflect a similar trend as obtained in experiments, with theoretical $k_{ISC} = 4.73 \times 10^{10}$ s^{-1} in DMICE-Br_2 and 4.13×10^{11} s^{-1} in DMICE-Br_3. Trajectory analysis from surface hopping simulations also reveals that the population follows the $S_1 \rightarrow T_{2,3} \rightarrow T_1$ pathway for DMICE-Br_2 as well as DMICE-Br_3. In conclusion, this work highlights the pivotal role of the number of bromine atoms in tuning the intersystem crossing dynamics in multi-brominated eumelanin derivatives, potentially paving the way for eumelanin-inspired photosensitizers for practical applications.

Data availability

All experimental and theoretical procedures, along with the supporting data are available in the ESI.†

Conflicts of interest

The authors have no conflicts of interest to declare.

Acknowledgements

M. H. acknowledges the Science and Engineering Research Board (CRG/2023/005859), Department of Science and Technology, Government of India, for financial support. K. V. acknowledges CSIR for financial assistance. D. T. acknowledges INSPIRE for financial support. We thank Mr Alex P. Andrews for the X-ray diffraction analyses. We thank Dr Sebastian Mai and Mr Sreekumar P. Y. for their support on the calculations with SHARC. We thank the Padmanabha HPC cluster at IISER TVM for the computing time.

References

1 C. M. Marian, Understanding and Controlling Intersystem Crossing in Molecules, *Annu. Rev. Phys. Chem.*, 2021, **72**, 617–640.
2 D. Sasikumar, A. T. John, J. Sunny and M. Hariharan, Access to the triplet excited states of organic chromophores, *Chem. Soc. Rev.*, 2020, **49**, 6122–6140.
3 M. R. Detty, S. L. Gibson and S. J. Wagner, Current clinical and preclinical photosensitizers for use in photodynamic therapy, *J. Med. Chem.*, 2004, **47**, 3897–3915.
4 M. Richter, S. Mai, P. Marquetand and L. González, Ultrafast intersystem crossing dynamics in uracil unravelled by ab initio molecular dynamics, *Phys. Chem. Chem. Phys.*, 2014, **16**, 24423–24436.
5 Y. Harada, C. Okabe, T. Kobayashi, T. Suzuki, T. Ichimura, N. Nishi and Y.-Z. Xu, Triplet Formation of 4-Thiothymidine and Its Photosensitization to Oxygen Studied by Time-Resolved Thermal Lensing Technique, *J. Phys. Chem. Lett.*, 2010, **1**, 480–484.
6 H. Kuramochi, T. Kobayashi, T. Suzuki and T. Ichimura, Photophysical properties of 5-substituted 2-thiopyrimidines, *J. Phys. Chem. B*, 2010, **114**, 8782–8789.
7 S. Mai, M. Pollum, L. Martínez-Fernández, N. Dunn, P. Marquetand, I. Corral, C. E. Crespo-Hernández and L. González, The origin of efficient triplet state population in sulfur-substituted nucleobases, *Nat. Commun.*, 2016, **7**, 13077.
8 F. Peccati, S. Mai and L. González, Insights into the deactivation of 5-bromouracil after ultraviolet excitation, *Philos. Trans. R. Soc., A*, 2017, **375**, 20160202.
9 M. Richter, P. Marquetand, J. González-Vázquez, I. Sola and L. González, Femtosecond Intersystem Crossing in the DNA Nucleobase Cytosine, *J. Phys. Chem. Lett.*, 2012, **3**, 3090–3095.
10 M. Barbatti, A. J. Aquino, J. J. Szymczak, D. Nachtigallová, P. Hobza and H. Lischka, Relaxation mechanisms of UV-photoexcited DNA and RNA nucleobases, *Proc. Natl. Acad. Sci. U. S. A.*, 2010, **107**, 21453–21458.
11 D. Valverde, S. Mai, A. V. Sanches de Araújo, S. Canuto, L. González and A. C. Borin, On the population of triplet states of 2-seleno-thymine, *Phys. Chem. Chem. Phys.*, 2021, **23**, 5447–5454.
12 Y.-H. Zhu, X.-F. Tang, X.-P. Chang, T.-S. Zhang, B.-B. Xie and G. Cui, Mechanistic Photophysics of Tellurium-Substituted Uracils: Insights from Multistate Complete-Active-Space Second-Order Perturbation Calculations, *J. Phys. Chem. A*, 2021, **125**, 8816–8826.
13 E. Vos, T. R. Scott, J. González-Vázquez, I. Corral, D. G. Truhlar and L. Gagliardi, Intrastrand Photolesion Formation in Thio-Substituted DNA: A Case Study Including Single-Reference and Multireference Methods, *J. Phys. Chem. A*, 2020, **124**, 10422–10433.
14 Z. Lan, Y. Lu, E. Fabiano and W. Thiel, QM/MM Nonadiabatic Decay Dynamics of 9H-Adenine in Aqueous Solution, *ChemPhysChem*, 2011, **12**, 1989–1998.
15 X. Guo, Y. Zhao and Z. Cao, A QM/MM MD insight into photodynamics of hypoxanthine: distinct nonadiabatic decay behaviors between keto-N7H and keto-N9H tautomers in aqueous solution, *Phys. Chem. Chem. Phys.*, 2014, **16**, 15381–15388.
16 R. Borrego-Varillas, D. C. Teles-Ferreira, A. Nenov, I. Conti, L. Ganzer, C. Manzoni, M. Garavelli, A. Maria de Paula and G. Cerullo, Observation of the Sub-100 Femtosecond Population of a Dark State in a Thiobase Mediating Intersystem Crossing, *J. Am. Chem. Soc.*, 2018, **140**, 16087–16093.
17 K. M. Farrell, M. M. Brister, M. Pittelkow, T. I. Sølling and C. E. Crespo-Hernández, Heavy-Atom-Substituted Nucleobases in Photodynamic Applications: Substitution of Sulfur with Selenium in 6-Thioguanine Induces a Remarkable Increase in the Rate of Triplet Decay in 6-Selenoguanine, *J. Am. Chem. Soc.*, 2018, **140**, 11214–11218.
18 D. Valverde, S. Mai, S. Canuto, A. C. Borin and L. González, Ultrafast Intersystem Crossing Dynamics of 6-Selenoguanine in Water, *JACS Au*, 2022, **2**, 1699–1711.
19 M. d'Ischia, A. Napolitano, A. Pezzella, P. Meredith and M. Buehler, Melanin Biopolymers: Tailoring Chemical Complexity for Materials Design, *Angew. Chem., Int. Ed.*, 2020, **59**, 11196–11205.
20 M. d'Ischia, A. Napolitano, A. Pezzella, P. Meredith and T. Sarna, Chemical and Structural Diversity in Eumelanins: Unexplored Bio-Optoelectronic Materials, *Angew. Chem., Int. Ed.*, 2009, **48**, 3914–3921.
21 D. Sasikumar, K. Vinod, J. Sunny and M. Hariharan, Exciton interactions in helical crystals of a hydrogen-bonded eumelanin monomer, *Chem. Sci.*, 2022, **13**, 2331–2338.
22 K. Vinod, R. Mathew, C. Jandl, B. Thomas and M. Hariharan, Electron diffraction and solid-state NMR reveal the structure and exciton coupling in a eumelanin precursor, *Chem. Sci.*, 2024, **15**, 16015–16024.
23 K. Vinod, S. D. Jadhav and M. Hariharan, Room Temperature Phosphorescence in Crystalline Iodinated Eumelanin Monomer, *Chem. – Eur. J.*, 2024, **30**, e202400499.
24 W. Cao, N. C. McCallum, Q. Z. Ni, W. Li, H. Boyce, H. Mao, X. Zhou, H. Sun, M. P. Thompson, C. Battistella, M. R. Wasielewski, A. Dhinojwala, M. D. Shawkey, M. D. Burkart, Z. Wang and N. C. Gianneschi, An Abiotic Selenium Analogue of Pheomelanin, *J. Am. Chem. Soc.*, 2020, **142**, 12802–12810.
25 Z. E. Siwicka, F. A. Son, C. Battistella, M. H. Moore, J. Korpanty, N. C. McCallum, Z. Wang, B. J. Johnson, O. K. Farha and N. C. Gianneschi, Synthetic Porous Melanin, *J. Am. Chem. Soc.*, 2021, **143**, 3094–3103.
26 B. Ashwood, M. Pollum and C. E. Crespo-Hernández, Photochemical and Photodynamical Properties of Sulfur-Substituted Nucleic Acid Bases, *Photochem. Photobiol.*, 2019, **95**, 33–58.
27 M. Zhu, H. Zhang, G. Ran, Y. Yao, Z.-S. Yang, Y. Ning, Y. Yu, R. Zhang, X.-X. Peng, J. Wu, Z. Jiang, W. Zhang, B.-W. Wang, S. Gao and J.-L. Zhang, Bioinspired Design of

seco-Chlorin Photosensitizers to Overcome Phototoxic Effects in Photodynamic Therapy, *Angew. Chem., Int. Ed.*, 2022, **61**, e202204330.

28 J. Sivanarayanan, E. Sebastian, K. Vinod, F. Würthner and M. Hariharan, Ultrafast Intersystem Crossing in Selenium-Annulated Perylene Bisimide, *J. Phys. Chem. C*, 2022, **126**, 13319–13326.

29 E. Sebastian, A. M. Philip, A. Benny and M. Hariharan, Null Exciton Splitting in Chromophoric Greek Cross (+) Aggregate, *Angew. Chem., Int. Ed.*, 2018, **57**, 15696–15701.

30 A. Mohan, E. Sebastian, M. Gudem and M. Hariharan, Near-Quantitative Triplet State Population via Ultrafast Intersystem Crossing in Perbromoperylenediimide, *J. Phys. Chem. B*, 2020, **124**, 6867–6874.

31 A. H. Aebly, J. N. Levy, B. J. Steger, J. C. Quirke and J. M. Belitsky, Expedient synthesis of eumelanin-inspired 5,6-dihydroxyindole-2-carboxylate ethyl ester derivatives, *RSC Adv.*, 2018, **8**, 28323–28328.

32 M. A. Spackman and D. Jayatilaka, Hirshfeld surface analysis, *CrystEngComm*, 2009, **11**, 19–32.

33 P. R. Spackman, M. J. Turner, J. J. McKinnon, S. K. Wolff, D. J. Grimwood, D. Jayatilaka and M. A. Spackman, CrystalExplorer: a program for Hirshfeld surface analysis, visualization and quantitative analysis of molecular crystals, *J. Appl. Crystallogr.*, 2021, **54**, 1006–1011.

34 R. M. Parrish, L. A. Burns, D. G. A. Smith, A. C. Simmonett, A. E. DePrince, E. G. Hohenstein, U. Bozkaya, A. Y. Sokolov, R. Di Remigio, R. M. Richard, J. F. Gonthier, A. M. James, H. R. McAlexander, A. Kumar, M. Saitow, X. Wang, B. P. Pritchard, P. Verma, H. F. Schaefer, K. Patkowski, R. A. King, E. F. Valeev, F. A. Evangelista, J. M. Turney, T. D. Crawford and C. D. Sherrill, Psi4 1.1: An Open-Source Electronic Structure Program Emphasizing Automation, Advanced Libraries, and Interoperability, *J. Chem. Theory Comput.*, 2017, **13**, 3185–3197.

35 P. Hobza and J. Řezáč, Introduction: Noncovalent Interactions, *Chem. Rev.*, 2016, **116**, 4911–4912.

36 T. Lu and F. Chen, Multiwfn: A multifunctional wavefunction analyzer, *J. Comput. Chem.*, 2012, **33**, 580–592.

37 A. M. Philip, M. Gudem, E. Sebastian and M. Hariharan, Decoding the Curious Tale of Atypical Intersystem Crossing Dynamics in Regioisomeric Acetylanthracenes, *J. Phys. Chem. A*, 2019, **123**, 6105–6112.

38 S. Sarkar, H. P. Hendrickson, D. Lee, F. DeVine, J. Jung, E. Geva, J. Kim and B. D. Dunietz, Phosphorescence in Bromobenzaldehyde Can Be Enhanced through Intramolecular Heavy Atom Effect, *J. Phys. Chem. C*, 2017, **121**, 3771–3777.

39 A. Ilina, K. E. Thorn, P. A. Hume, I. Wagner, R. R. Tamming, J. J. Sutton, K. C. Gordon, S. K. Andreassend, K. Chen and J. M. Hodgkiss, The photoprotection mechanism in the black-brown pigment eumelanin, *Proc. Natl. Acad. Sci. U. S. A.*, 2022, **119**, e2212343119.

40 S. Freed and W. Salmre, Phosphorescence Spectra and Analyses of Some Indole Derivatives, *Science*, 1958, **128**, 1341–1342.

41 M. A. Niyas, S. Garain, K. Shoyama and F. Würthner, Room-Temperature Near-Infrared Phosphorescence from C64 Nanographene Tetraimide by π-Stacking Complexation with Platinum Porphyrin, *Angew. Chem., Int. Ed.*, 2024, **63**, e202406353.

42 F. Plasser, S. Gómez, M. F. S. J. Menger, S. Mai and L. González, Highly efficient surface hopping dynamics using a linear vibronic coupling model, *Phys. Chem. Chem. Phys.*, 2019, **21**, 57–69.

43 S. Mai, D. Avagliano, M. Heindl, P. Marquetand, M. F. S. J. Menger, M. Oppel, F. Plasser, S. Polonius, M. Ruckenbauer, Y. Shu, D. G. Truhlar, L. Zhang, P. Zobel and L. González, *SHARC3.0: Surface Hopping Including Arbitrary Couplings – Program Package for Non-Adiabatic Dynamics*, 2023, **https://sharc-md.org/**.

44 M. Richter, P. Marquetand, J. González-Vázquez, I. Sola and L. González, SHARC: ab Initio Molecular Dynamics with Surface Hopping in the Adiabatic Representation Including Arbitrary Couplings, *J. Chem. Theory Comput.*, 2011, **7**, 1253–1258.

45 J. P. Zobel, M. Heindl, F. Plasser, S. Mai and L. González, Surface Hopping Dynamics on Vibronic Coupling Models, *Acc. Chem. Res.*, 2021, **54**, 3760–3771.

46 A. J. Atkins and L. González, Trajectory Surface-Hopping Dynamics Including Intersystem Crossing in $[Ru(bpy)_3]^{2+}$, *J. Phys. Chem. Lett.*, 2017, **8**, 3840–3845.

47 P. J. Stephens, F. J. Devlin, C. F. Chabalowski and M. J. Frisch, Ab Initio Calculation of Vibrational Absorption and Circular Dichroism Spectra Using Density Functional Force Fields, *J. Phys. Chem.*, 1994, **98**, 11623–11627.

48 F. Neese, Software update: The ORCA program system—Version 5.0, *Wiley Interdiscip. Rev.: Comput. Mol. Sci.*, 2022, **12**, e1606.

49 Y. Takano and K. N. Houk, Benchmarking the Conductor-like Polarizable Continuum Model (CPCM) for Aqueous Solvation Free Energies of Neutral and Ionic Organic Molecules, *J. Chem. Theory Comput.*, 2005, **1**, 70–77.

50 S. Mai, M. Menger, M. Marazzi, D. L. Stolba, A. Monari and L. González, Competing ultrafast photoinduced electron transfer and intersystem crossing of $[Re(CO)_3(Dmp)(His124)(Trp122)]^+$ in Pseudomonas aeruginosa azurin: a nonadiabatic dynamics study, *Theor. Chem. Acc.*, 2020, **139**, 65.

51 S. Grimme, S. Ehrlich and L. Goerigk, Effect of the damping function in dispersion corrected density functional theory, *J. Comput. Chem.*, 2011, **32**, 1456–1465.

52 S. Mai, P. Marquetand and L. González, Nonadiabatic dynamics: The SHARC approach, *Wiley Interdiscip. Rev.: Comput. Mol. Sci.*, 2018, **8**, e1370.

53 J. P. Dahl and M. Springborg, The Morse oscillator in position space, momentum space, and phase space, *J. Chem. Phys.*, 1988, **88**, 4535–4547.

54 J. C. Tully and R. K. Preston, Trajectory Surface Hopping Approach to Nonadiabatic Molecular

Collisions: The Reaction of H+ with D2, *J. Chem. Phys.*, 1971, **55**, 562–572.

55 S. Mai, P. Marquetand and L. González, A general method to describe intersystem crossing dynamics in trajectory surface hopping, *Int. J. Quantum Chem.*, 2015, **115**, 1215–1231.

56 M. Fumanal, F. Plasser, S. Mai, C. Daniel and E. Gindensperger, Interstate vibronic coupling constants between electronic excited states for complex molecules, *J. Chem. Phys.*, 2018, **148**, 124119.

57 G. Granucci, M. Persico and A. Toniolo, Direct semiclassical simulation of photochemical processes with semiempirical wave functions, *J. Chem. Phys.*, 2001, **114**, 10608–10615.

58 F. Plasser, M. Ruckenbauer, S. Mai, M. Oppel, P. Marquetand and L. González, Efficient and Flexible Computation of Many-Electron Wave Function Overlaps, *J. Chem. Theory Comput.*, 2016, **12**, 1207–1219.

59 A. Jain, E. Alguire and J. E. Subotnik, An Efficient, Augmented Surface Hopping Algorithm That Includes Decoherence for Use in Large-Scale Simulations, *J. Chem. Theory Comput.*, 2016, **12**, 5256–5268.

60 J. Cao and Z.-Z. Xie, Internal conversion and intersystem crossing in α,β-enones: a combination of electronic structure calculations and dynamics simulations, *Phys. Chem. Chem. Phys.*, 2016, **18**, 6931–6945.

61 A. Malinge, S. Kumar, D. Chen, E. Zysman-Colman and S. Kéna-Cohen, Heavy Atom Effect in Halogenated mCP and Its Influence on the Efficiency of the Thermally Activated Delayed Fluorescence of Dopant Molecules, *J. Phys. Chem. C*, 2024, **128**, 1122–1130.